Computers and Concrete, *Vol. 21, No. 6 (2018) 727-739*
DOI: https://doi.org/10.12989/cac.2018.21.6.727

Morphological segmentation based on edge detection-II for automatic concrete crack measurement

Tung-Ching Su[1a] and Ming-Der Yang[*2]

[1]*Department of Civil Engineering and Engineering Management, National Quemoy University, Kinmen, Taiwan*
[2]*Department of Civil Engineering, and Innovation and Development Center of Sustainable Agriculture, National Chung Hsing University, Taichung City, Taiwan*

(Received November 24, 2017, Revised February 27, 2018, Accepted March 23, 2018)

Abstract. Crack is the most common typical feature of concrete deterioration, so routine monitoring and health assessment become essential for identifying failures and to set up an appropriate rehabilitation strategy in order to extend the service life of concrete structures. At present, image segmentation algorithms have been applied to crack analysis based on inspection images of concrete structures. The results of crack segmentation offering crack information, including length, width, and area is helpful to assist inspectors in surface inspection of concrete structures. This study proposed an algorithm of image segmentation enhancement, named morphological segmentation based on edge detection-II (MSED-II), to concrete crack segmentation. Several concrete pavement and building surfaces were imaged as the study materials. In addition, morphological operations followed by cross-curvature evaluation (CCE), an image segmentation technique of linear patterns, were also tested to evaluate their performance in concrete crack segmentation. The result indicates that MSED-II compared to CCE can lead to better quality of concrete crack segmentation. The least area, length, and width measurement errors of the concrete cracks are 5.68%, 0.23%, and 0.00%, respectively, that proves MSED-II effective for automatic measurement of concrete cracks.

Keywords: concrete crack; aging concrete; cracking; morphological segmentation; edge detection

1. Introduction

Most infrastructures are currently constructed of concrete or reinforced concrete, but aging and deterioration with time are the most serious problems in maintenance during the service life (Yang and Su 2006, Yang and Su 2007), especially for green buildings (Yang *et al.* 2017). As the most common and typical feature of concrete aging and deterioration, a crack in concrete structures appears in various patterns, including micro-crack, separate crack, bending crack, shearing crack, shrinkage crack, interstitial crack, longitudinal crack, and surface crack (Chen *et al.* 2017). Among these types of cracks, structural cracks, such as separate crack, bending crack, or shearing crack, usually have a great impact on the health of concrete structures. Routine monitoring and health assessment are essential for revealing failures and to put forth an appropriate rehabilitation strategy extending the service life of concrete structures.

Health monitoring and assessment on concrete structures are traditionally implemented by human eyes, but manual inspection is sometimes time-consuming or dangerous when the inspected area is enormous or the inspected site is difficult to get at. In the last decade, several non-destructive testing and evaluation methods have been presented to assist human inspection in the health assessment of concrete structures. A variety of numerical models have been developed to predict concrete crack damage for concrete structures (Belletti *et al.* 2017, Yang *et al.* 2017). Terrestrial Laser Scanning as an active approach was effectively used in diagnostics of reinforced concrete elements to virtually reconstruct failure process, measure geometry, and assess a condition of structure (Janowski *et al.* 2016). However, this approach is relatively expensive and technique-dependent. Alternatively, imaging systems have been developed to assist eyesight with low-cost and easy-operation in the inspection on various objects, such as bridges (Tung *et al.* 2002, Metni and Hamel 2007, Oh *et al.* 2009, Zhu *et al.* 2010, Yang *et al.* 2011a, Riveiro *et al.* 2012), pavement (Pan *et al.* 2011), underground pipes (Gokhale and Graham 2004, Iyer and Sinha 2005, Sinha and Fieguth 2006, Yang and Su 2008, Yang and Su 2009, Mashford *et al.* 2010, Su and Yang 2014, Yang *et al.* 2017), and tunnels (Yu *et al.* 2007, Wang *et al.* 2009, Victores *et al.* 2011). The utility of the imaging systems focuses on identifying and diagnosing cracks in concrete structures through image processing. Yu *et al.* (2007) established a crack detection system to semi-automatically detect concrete cracks in a tunnel by crack segmentation. Oh *et al.* (2009) developed an automated bridge inspection system, in which a morphological operation and a crack tracing algorithm were applied to crack detection and measurement with a detection rate of 96.7% and an average error of 0.023 mm for crack widths in good environmental conditions. However, correct crack morphology segmentation is usually difficult due to image luminance, image contrast, image

∗Corresponding author, Distinguished Professor
E-mail: mdyang@nchu.edu.tw
[a]Associate Professor

ISSN: 1598-8198 (Print), 1598-818X (Online)

noise, and environmental influence (Yang *et al.* 2011b, Su *et al.* 2011).

To reduce the environmental influence of lighting not being evenly distributed on inspected objects, a novel edge detection algorithm using mathematical morphology has been proposed to segment crack morphologies in the dark regions in images and proven to be an efficient solution as a machine vision application (Chen *et al.* 2002). Iyer and Sinha (2005) presented a robust approach for automatic detection and segmentation of cracks in underground pipeline images by adopting a morphological operation coupled with curvature evaluation for crack segmentation with an accuracy of 98.0%. The morphological approach, consisting of opening operations, was demonstrated to be effective for dealing with underground pipe images having varying background patterns and non-uniform illuminations (Sinha and Fieguth 2006). In addition, Lee *et al.* (2006) developed a machine vision algorithm, including noise elimination, crack network mapping and modeling, and path planning for pavement crack sealing, with an accuracy of over 86%. Charge Coupled Device (CCD) cameras have been employed to segment cracks from a noisy background system for bridge crack inspection (Tung *et al.* 2002, Oh *et al.* 2009) and tunnel crack detection (Yu *et al.* 2007).

The above studies conclude that segmenting cracks in concrete structures from noisy environments is a challenge for the development of machine vision systems. Based on the SSET (sewer scanner evaluation technology) images with favorable illuminance and contrast, Iyer and Sinha (2005) reached the optimal accuracy of crack segmentation up to 98.0%, after cracks were first enhanced by a mathematical morphology with respect to spatial property and cross-curvature evaluation (CCE) was then performed to segment cracks from analogous background patterns. This paper proposes a modified morphological segmentation approach using edge detection to reduce the requirement for specific imaging devices, and tests CCE to see the performance of concrete crack segmentation on common digital images, which are much more available but usually inferior to SSET images in illuminance or contrast.

2. Background of crack segmentation algorithms

Automated inspection at present is expected to replace manual inspection for detecting cracks in concrete structures. Thus, Su *et al.* (2011) presented an algorithm of image segmentation enhancement, the so-called morphological segmentation based on edge detection (MSED), for segmenting sewer pipe defects and indicated that MSED is effective at morphology enhancement for typical sewer pipe defects. Furthermore, Su (2013, 2015) and Su and Yang (2014) also applied the MSED technique to crack segmentations.

A weighted median filter in the MSED technique is first introduced to smooth out any details of a noisy environment and to maintain crack texture. Second, edge detection is applied to the filtered image to obtain a binary image, in which the value of the edge pixel of the region of interest (ROI) is marked by "1". However, ROI might or might not be enclosed by detected edges. Thus, based on the edge detection result, MSED not only encloses ROI, but also preserves the original morphology of ROI.

A crack fragmentary connection is a common task in crack recognition applications (Yun *et al.* 2015). However, MSED cannot connect fragmentary segmented image regions that influence the completeness of ROI. In order to overcome the problem, based on the concept of MSED this paper proposed another algorithm of image segmentation enhancement, named MSED-II, where background space between any neighbor segmented image regions is transformed into ROI to attempt to strengthen the completeness of ROI, i.e., the image region of a true crack. When operating MSED-II, preserving the correctness of ROI is also expected. Finally, three indices, including completeness, correctness, and quality, were introduced into the performance estimation of crack segmentation. The crack segmentation performances of MSED-II and CCE were also compared and discussed.

3. Experimental materials

Cracks on concrete structure surfaces were imaged by a common digital camera, whose specifications are 3.15 M (1536×2048) pixels and adjustable focal lengths of 35 mm through 105 mm. Su (2013) considered that the characteristics of sunlight projected onto horizontal and vertical concrete surfaces are different if no accessory light is applied. Su (2013) acquired 100 inspection images of a concrete pavement as the experimental materials. Half of the 100 inspection images had a crack pattern and the other half did not, i.e., showing a clear pattern. Moreover, 33 inspection images of a concrete building were also taken as the experimental materials. Seventeen of the 33 inspection images exhibit a crack pattern and the residuals do not. The experimental result approached an optimal accuracy of 90% for crack image registration. This research furthermore selected 24 inspection images registered as crack images by Su (2013), of the concrete pavement and building surfaces, and the object distances of the inspection images are about 0.3 to 0.5 m (see Figs. 1 and 2).

4. Methodology

The scheme of this research is shown as Fig. 3. In the beginning, a crack image is transformed into gray level one, because the image tone of a crack is almost darker than its neighborhood. In other words, color information is unimportant and is not considered in this research. The preprocessing of MSED-II involves weighted median filtering, image opening, and binary transformation using Otsu's technique. According to Iyer and Sinha (2005), the preprocessing of CCE includes weighted median filtering and line-based structure determination. Using CCE prior to concrete crack segmentation, crack morphology in a filtered image needs to be enhanced by a series of morphological operations, including image closing, image reconstruction, image subtraction, and image addition, which are executed from 0° to 180° stepped by 10° (Iyer and Sinha 2005). With a Laplacian filter having a linear type of 12 elements with

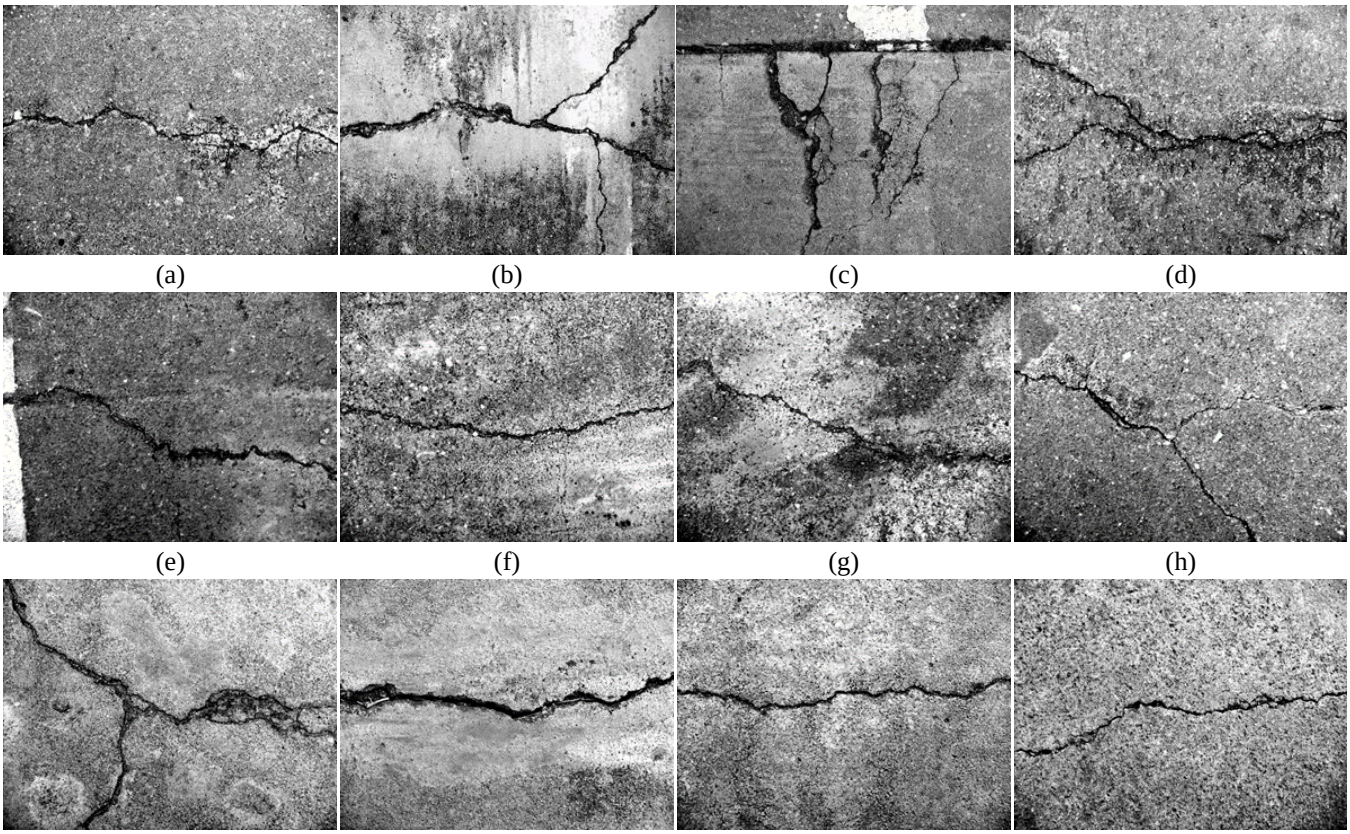

(a) (b) (c) (d)

(e) (f) (g) (h)

(i) (j) (k) (l)

Fig. 1 Crack images of a concrete pavement

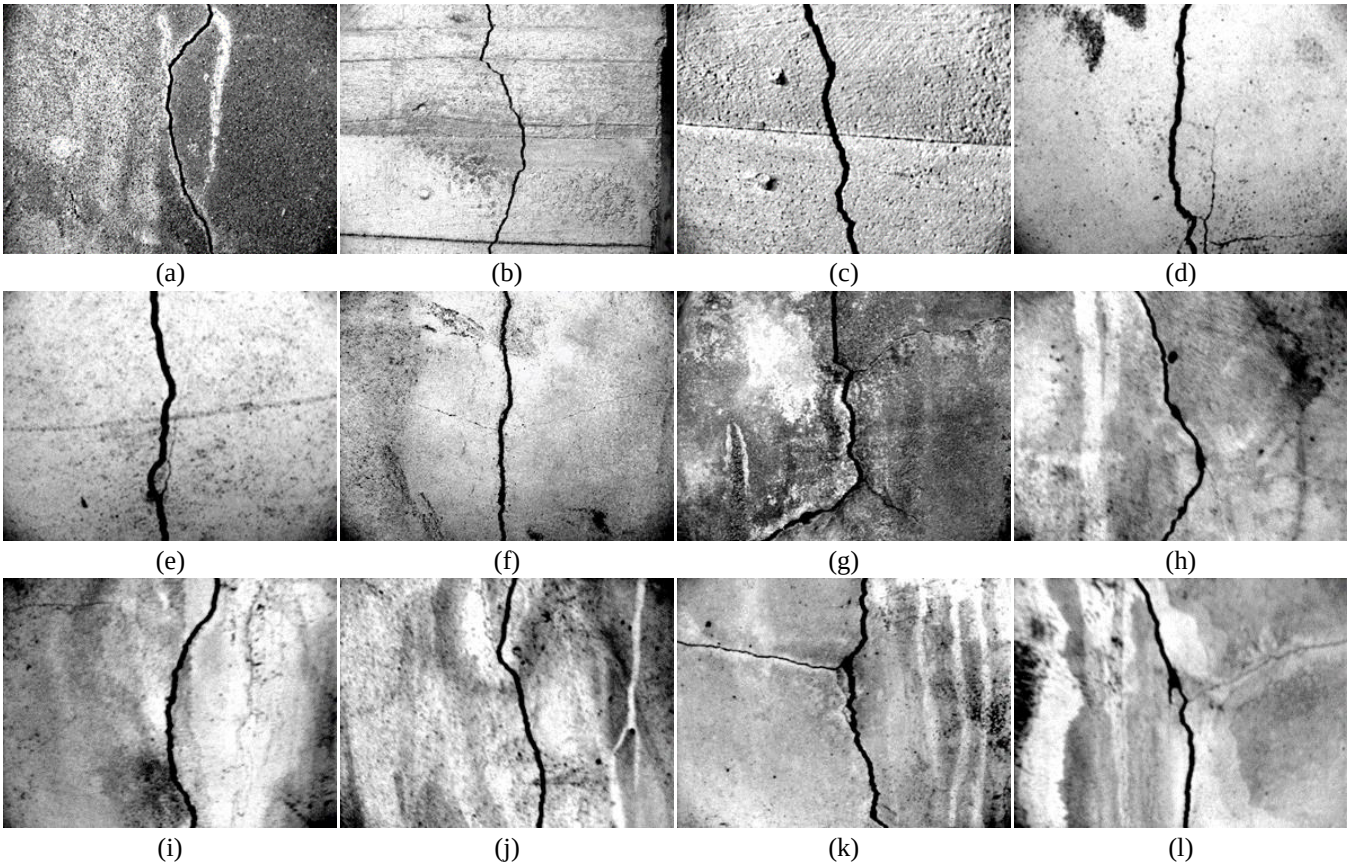

(a) (b) (c) (d)

(e) (f) (g) (h)

(i) (j) (k) (l)

Fig. 2 Crack images of a concrete building

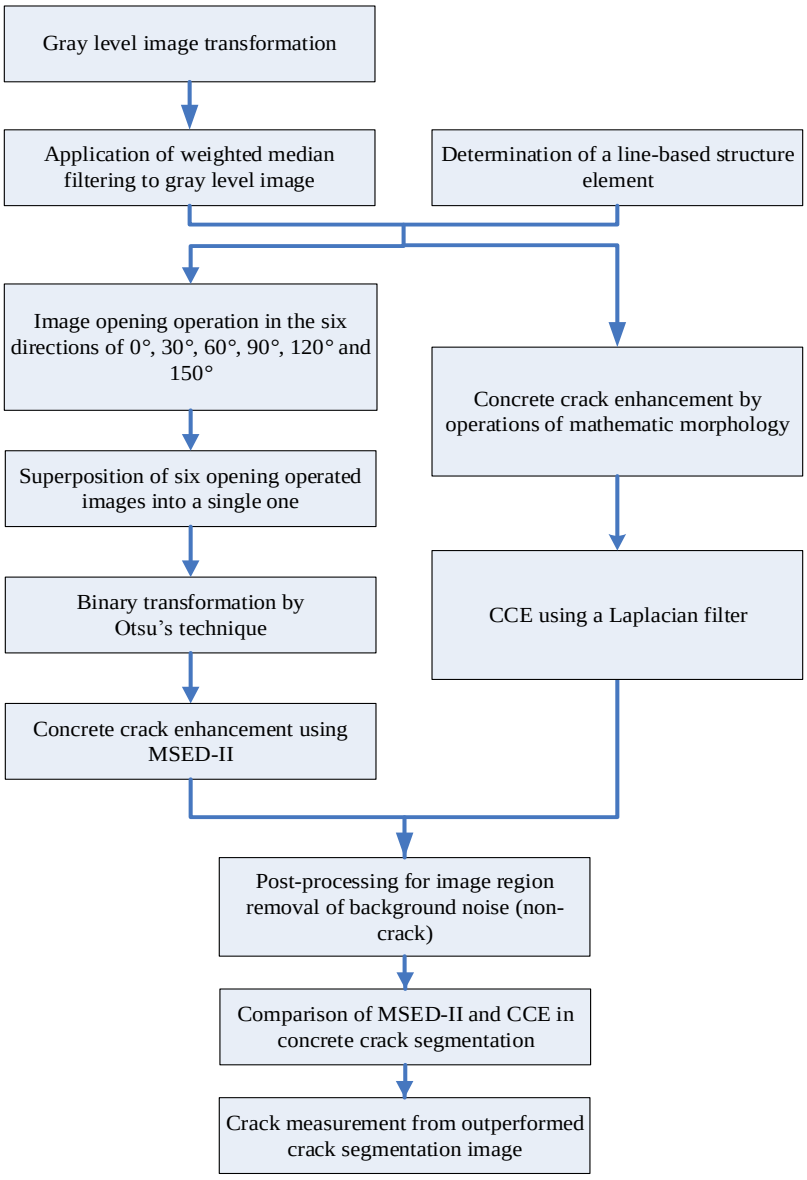

Fig. 3 Scheme of concrete crack segmentation

standard deviation (σ)=0.5, the image region with significant curvature can be extracted from the morphological operation image (Iyer and Sinha 2005).

Post-processing of removing segmented image regions, which belong to background noise (non-crack), from the segmentation result is necessary for accuracy improvement of crack image registration (Su 2013). Therefore, post-processing was also employed in this research. Between MSED-II and CCE, the outperformance segmentation was selected to measure the sizes (in pixels), including area, length, and width, of the segmented true crack. The contents of the preprocessing, MSED-II algorithm, and the post-processing are briefly described as follows.

4.1 Weighted median filtering

A weighted median filter, which is one type of smoothing filter and a modification of median filter, can remove environmental noise from an image as well as maintain textures of the image regions of interest (Wendt *et al.* 1986, Yli-Harja *et al.* 1991). Su (2013) applied a 5×5 weighted median filter to gray level images to effectively enhance cracks and reduce the interferences of noisy environments. Also, the different weight values given for the central position of a weighted median filter show no great impact on crack enhancement (Su 2013). Thus, this research gives the weight value at the central position of the weighted median filter as 5.

4.2 Image opening

This research adopted image opening, where an erosion of an image is followed by a dilation of the eroded result (Shih 2010), to enhance the image regions. Due to the morphological characteristic of an irregular line-like crack, a linear structural element of 15 pixels was introduced into the operation of image opening in six directions, including 0°, 30°, 60°, 90°, 120°, and 150°, to enhance all cracks

irrespective of their orientations. Thus, an inspection image obtains six opening operated images in the format of a gray level. Overlapping the six images into a single one leads to a final opening operated image.

4.3 Otsu's technique

Otsu's technique based on discriminant analysis helps determine an optimal threshold for binary transformation (Yan 1996). After binary transformation using Otsu's technique, the difference between light and dark image regions can be maximized, and the difference within either light or dark image regions can also be minimized.

4.4 MSED-II algorithm

MSED was first presented by Su *et al.* (2011) and applied to the segmentation of sewer pipe defects in the inspection images. Edge detection is considered as an important pre-processing step in image segmentation (Chen *et al.* 2002). Intuitionally, based on performances of edge detection MSED was designed to attempt to enhance the correct morphologies of infrastructure defects from inspection images (Su *et al.* 2011). In MSED, a region growing by 4-neighborhood connection is implemented within a ROI to transform the background pixels into the ROI. In MSED-II, however, the region growing is based on an 8-neighborhood connection and implemented between any neighbor ROIs to transform fragmentary ROIs into intact ones. Thus, this research rewrote MSED as MSED-II, and the MSED-II algorithm is shown as follows.

1**begin initialize** pixel numbers of inspection image in the row m and column n directions, detected distance d, $d \leftarrow 1$, image region $\mathbf{R}$ with logical value as 1 in binary image
2 **for** $d \leftarrow d + 1$
3 **for** $i \leftarrow i + 1$ *%Loop I for horizontal crack detection*
4 **for** $j \leftarrow j + 1$
5 **if** $\mathbf{R}_{ij}$ **and** $\mathbf{R}_{i(j+d)} \in 1$ **then** $\{\mathbf{R}_{i(j+1)}, \ldots, \mathbf{R}_{i(j+d-1)}\} \leftarrow 1$
6 **until** $j = n - d$
7 **until** $i = m$
8**for** $j \leftarrow j + 1$ *% Loop II for vertical crack detection*
9 **for** $i \leftarrow i + 1$
10 **if** $\mathbf{R}_{ij}$ **and** $\mathbf{R}_{(i+d)j} \in 1$ **then** $\{\mathbf{R}_{(i+1)j}, \ldots, \mathbf{R}_{(i+d-1)j}\} \leftarrow 1$
11 **until** $i = m - d$
12**until** $j = n$
13**for** $i \leftarrow i + 1$ *% Loop III for diagonal crack detection at 45°*
14 **for** $j \leftarrow j + 1$
15 **if** $\mathbf{R}_{ij}$ **and** $\mathbf{R}_{(i+d)(j+d)} \in 1$ **then** $\{\mathbf{R}_{(i+1)(j+1)}, \ldots, \mathbf{R}_{(i+d-1)(j+d-1)}\} \leftarrow 1$
16 **until** $j = n - d$
17**until** $i = m - d$
18**initialize** $j \leftarrow n$
19**for** $j \leftarrow j - 1$ *% Loop IV for diagonal crack detection at 135°*
20 **for** $i \leftarrow i + 1$
21 **if** $\mathbf{R}_{ij}$ **and** $\mathbf{R}_{(i+d)(j-d)} \in 1$ **then** $\{\mathbf{R}_{(i+1)(j-d+1)}, \ldots, \mathbf{R}_{(i+d-1)(j-1)}\} \leftarrow 1$
22 **until** $i = m - d$
23**until** $j = 1 + d$
24**until** $\mathbf{R}_d = \mathbf{R}_{d-1}$
25**end**

In the beginning of the MSED-II algorithm, a detected distance d needs to be given, which represents the possible pixel distance between any neighbor ROIs. A kernel is employed to identify the edge pixels of ROIs, which are selected as the seeds of region growing. Due to the 8-neighborhood connection, the region growing is implemented at each seed pixel in the four directions, including 0°, 90°, 45°, and 135°. The detected distance d will be lengthened along with the iterative operation of MSED-II. If the segmentation result of this iteration is the same as that of the last iteration, then the iterative operation of MSED-II is terminated.

4.5 Postprocessing

After using MSED for image segmentation enhancement, unfortunately the image regions of non-defects will also be segmented (Su and Yang 2014). The number of segmented image regions of non-defects is sometimes so extremely enormous as to severely deteriorate the defect segmentation performance. In order to remove the image regions of non-cracks, post-processing determining the criteria of crack patterns was established by Su (2013), who also considered that a larger segmented image region, when compared with a smaller one, has a higher probability of showing a crack pattern. Su (2013) and Sun *et al.* (2016) also noted that a segmented image region with an eccentricity value approximating to 1 (line-like) would have a higher probability of being regarded as a crack pattern than that with an eccentricity value approximating to 0 (circle-like). If the morphological features, i.e. area and eccentricity, of a segmented image region do not satisfy the determination criterion, then the segmented image region is determined to be a non-crack pattern and removed from the segmentation result.

This research refers the post-processing for non-crack pattern removal to the determination criterion (Su 2013) - i.e., area threshold of $\geqq 50$ pixels coupled with eccentricity threshold of $\geqq 0.95$. The above determination criterion demonstrates its usefulness in crack image registration.

5. Experimental results and discussion

The crack segmentation performances of CCE and MSED-II is compared according to three indices: completeness, correction, and quality. Completeness (*Compl*) means the percentage of image regions of true cracks being segmented against those of true cracks interpreted by human eyes. Correctness (*Corr*) denotes the percentage of correctly segmented image regions of cracks

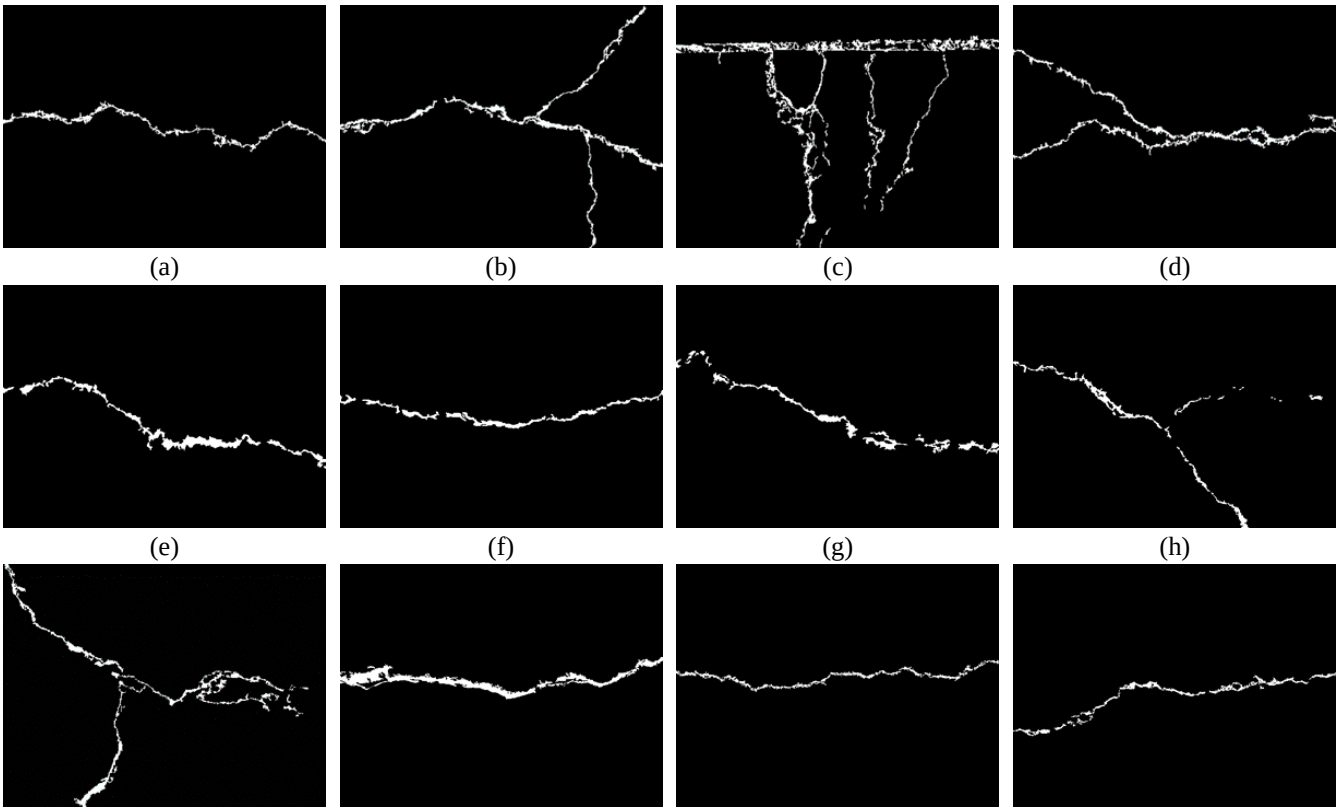

Fig. 4 Manual interpretation of true cracks for Fig. 1

against all segmented image regions. *Quality* is a general measurement combining *Compl* and *Corr* into a signal index. The calculations of *Compl*, *Corr*, and *Quality* are as follows:

$$Compl = (S_e \cap M_s) / M_s \quad (1)$$

$$Corr = (S_e \cap M_s) / S_e \quad (2)$$

$$Quality = (Compl \cdot Corr)/(Compl - Compl \cdot Corr + Corr) \quad (3)$$

where S_e represents the image segmentation result by MSED-II or CCE; and M_s expresses the image region of a true crack by manual interpretation. Figs. 4 and 5 show the manual interpretations of the true cracks for Figs. 1 and 2, respectively.

5.1 Crack segmentation result using MSED-II

The crack segmentation results using MSED-II are shown in Figs. 6 and 7. The segmented image regions are depicted in red polylines. The performances of MSED-II in the segmentations of the concrete pavement and building cracks are evaluated as Tables 1 and 2, respectively. Tables 1 and 2 present that the *Compl* values are usually higher than the *Corr* values. This result means that most image regions belonging to true cracks can be segmented by MSED-II. However, some image regions of background noises were also segmented and reserved after the post-processing.

In Table 1, Images a, e, g, h, k, and l exhibit that less than 50% of image regions of the true cracks were segmented. In other words, more than 50% of image regions segmented in the above binary images belong to background noises. Referring to Figs. 4 and 6, one can find that the segmented image regions of background noises have tones as deep as the true cracks. Unfortunately, the morphological features of the segmented image regions of background noises match the post-processing's threshold, so that the non-crack patterns were also reserved. Among the 12 inspection images, Images j and g obviously obtained the highest and lowest *Quality* values, respectively, and the other *Quality* values are approximately between 40% and 50%.

In Table 2, less than 50% of image regions of the true cracks were segmented in Images b, h, j, and l. Referring to Figs. 5 and 7, these four segmented images show that the sizes of the segmented image regions of background noises are much larger than or approximately equal to those of the true cracks. For instance, a large and strip-shaped image region, which belongs to background noise, was segmented on the right-hand side of Image b in Fig. 7 so that the *Corr* and *Quality* values were severely deteriorated. Some of the inspection images, such as Images c, e, and k, obtained higher *Corr* values than their corresponding *Compl* values. The common characteristic of the above three segmented images is that there were fewer image regions of background noises segmented. Among the 12 inspection images, Images c, d, and e obtained *Quality* values above 60%, and the other *Quality* values are also approximately between 40 and 50%. This paper demonstrated that MSED-

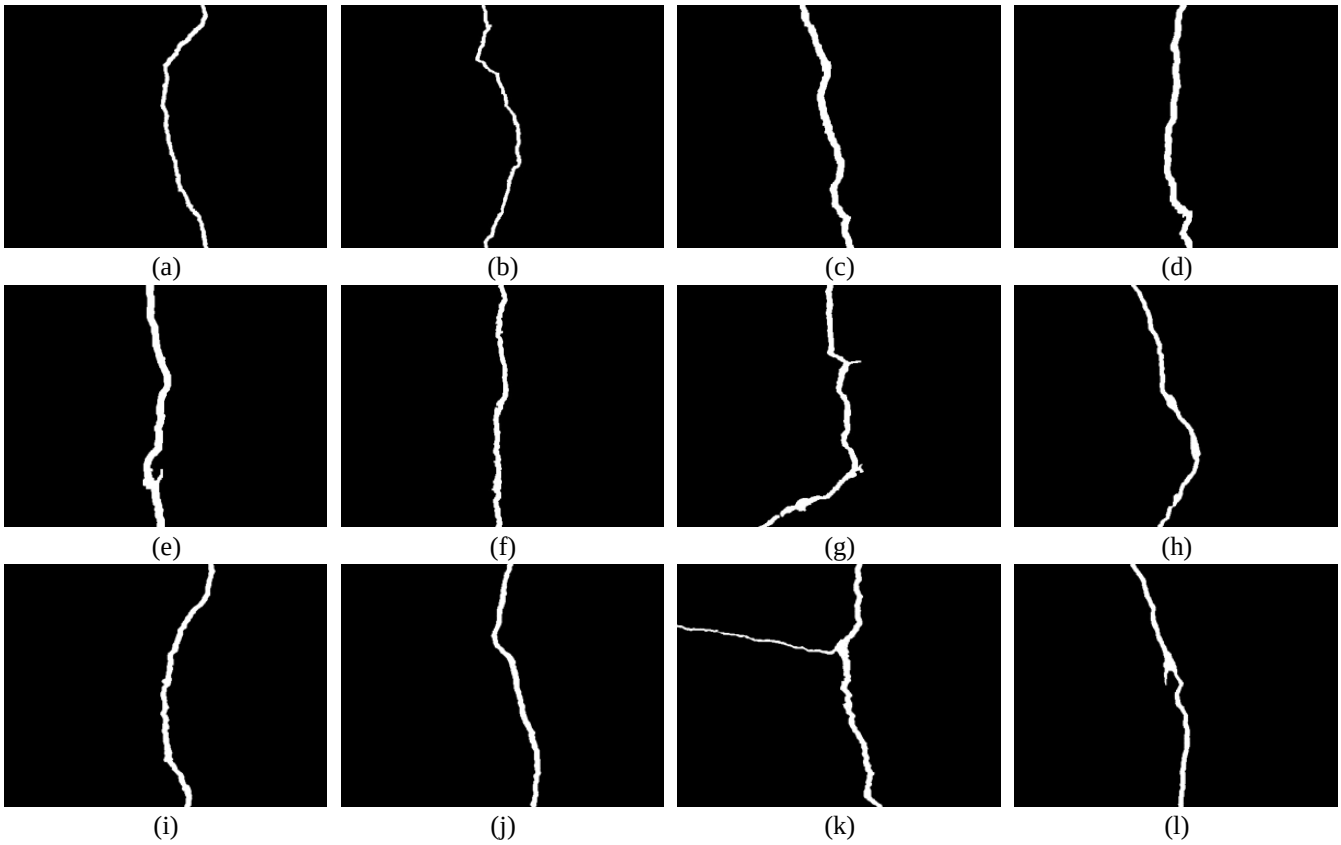

Fig. 5 Manual interpretation of true cracks for Fig. 2

II leads to similar crack segmentation performances between concrete pavement and buildings.

In Fig. 4, Images b, c, and i display the irregular cracks, so this paper additionally applied MSED to the crack segmentation and compared the performances of MSED with MSED-II. Nevertheless, the obtained *Quality* values by MSED are between 15% and 20%, much less 45% obtained by MSED-II. The inferior crack segmentation result of MSED majorly results from many background noise (non-crack) segmentations. Thus, this experiment demonstrates the necessity of developing MSED-II.

5.2 Crack segmentation result using CCE

The crack segmentation results using CCE are shown in Figs. 8 and 9. Tables 3 and 4 list the performance evaluations of CCE in segmenting the concrete pavement and building cracks, respectively. In Table 3, most of the binary images also have higher *Compl* values than *Corr* values, and half the *Compl* values are above 60%. Images c and g have the lowest *Compl* and *Corr* values, respectively. Only the 23.28% of true cracks in Image c were segmented, and about 80% of the segmented image regions in Image g belong to background noises. Thus, Images c and g both obtained lower *Quality* values than the other binary images. Conclusively, the obtained *Quality* values of applying CCE to concrete pavement crack segmentation are between 20 and 40%.

In Table 4, most of the binary images have higher *Corr* value than *Compl* values, running contrary to the segmentation performance shown as Table 3. Over half the binary images have *Corr* values above 60%. Even the *Corr* value of Image e reaches 90.45%. Images j and l obtained higher *Compl* values as well as *Corr* values approximating to 70%. Thus, the above two binary images have higher *Quality* values than the others. Table 4 also shows that the lowest *Corr* value of 28.33% was evaluated for Image b, because the lateral and deep stripe of wood moldboard was segmented by CCE (see Fig. 9(b)). The segmented stripe greatly deteriorates the segmentation correctness of the true crack, but this result demonstrates that CCE is sensitive to a line-like pattern so as to be useful in thin crack segmentation.

According to the *Quality* values in Tables 3 and 4, CCE has been demonstrated better in concrete buildings than pavement crack segmentation. Furthermore, the better performances mostly depend upon the correctness of crack segmentation. Half the binary images of the concrete building cracks have *Corr* values above 70%; however, the highest *Corr* value is merely 65.04% of those of the concrete pavement cracks.

5.3 Comparison of crack segmentation performances using MSED-II and CCE

A pair-wise comparison between MSED-II and CCE for *Compl*, *Corr*, and Quality is shown as Table 5, and the outperformance is symbolized by "√". In the concrete pavement crack segmentation, MSED-II compared to CCE is effective in segmenting complete as well as correct true

Table 1 Performance evaluation of MSED-II in concrete pavement crack segmentation

Image ID	Size of the image regions of the cracks (pixels)			*Compl* (%)	*Corr* (%)	*Quality* (%)
	M_s	S_e	$S_e \cap M_s$			
a	2438	3458	1483	60.83	42.89	33.61
b	4678	6159	3363	71.89	54.60	45.00
c	8171	9422	5685	69.58	60.34	47.74
d	4268	5446	3287	77.02	60.36	51.14
e	3689	7932	3414	92.55	43.04	41.60
f	2466	3385	1708	69.26	50.46	41.23
g	3052	5812	1676	54.91	28.84	23.32
h	2347	3702	1424	60.67	38.47	30.79
i	4445	5240	3023	68.01	57.69	45.38
j	4839	5650	4564	94.32	80.78	77.03
k	1822	3649	1638	89.90	44.89	42.73
l	2061	3749	1689	81.95	45.05	40.99

Table 2 Performance evaluation of MSED-II in concrete building crack segmentation

Image ID	Size of the image regions of the cracks (pixels)			*Compl* (%)	*Corr* (%)	*Quality* (%)
	M_s	S_e	$S_e \cap M_s$			
a	2971	3877	2010	67.65	51.84	41.55
b	2462	5497	1147	46.59	20.87	16.84
c	4634	3989	3742	80.75	93.81	76.66
d	4377	4361	3430	78.36	78.65	64.62
e	5123	4434	3998	78.04	90.17	71.92
f	3473	4526	2466	71.00	54.49	44.57
g	4555	5598	3627	79.63	64.79	55.58
h	3443	6555	2677	77.75	40.84	36.57
i	3857	5192	3166	82.08	60.98	53.82
j	3595	5492	2674	74.38	48.69	41.70
k	5039	4752	3390	67.28	71.34	52.96
l	3430	5779	2519	73.44	43.59	37.65

Table 3 Performance evaluation of CCE in concrete pavement crack segmentation

Image ID	Size of the image regions of the cracks (pixels)			*Compl* (%)	*Corr* (%)	*Quality* (%)
	M_s	S_e	$S_e \cap M_s$			
a	2438	4254	1545	63.37	36.32	30.02
b	4678	5932	2947	63.00	49.68	38.46
c	8171	3720	1902	23.28	51.13	19.04
d	4268	5801	2377	55.69	40.98	30.90
e	3689	1989	1235	33.48	62.09	27.80
f	2466	6683	1836	74.45	27.47	25.11
g	3052	6055	1256	41.15	20.74	16.00
h	2347	3347	1420	60.50	42.42	33.22
i	4445	4517	2239	50.37	49.57	33.30
j	4839	3304	2149	44.41	65.04	35.85
k	1822	3809	1397	76.67	36.67	32.99
l	2061	4906	1388	67.35	28.29	24.88

Table 4 Performance evaluation of CCE in concrete building crack segmentation

Image ID	Size of the image regions of the cracks (pixels)			*Compl* (%)	*Corr* (%)	*Quality* (%)
	M_s	S_e	$S_e \cap M_s$			
a	2971	2315	1298	43.69	56.07	32.55
b	2462	3939	1116	45.33	28.33	21.12
c	4634	6230	2782	60.03	44.65	34.42
d	4377	3983	2772	63.33	69.60	49.61
e	5123	2533	2291	44.72	90.45	42.70
f	3473	2808	2036	58.62	72.51	47.96
g	4555	3876	2144	47.07	55.31	34.10
h	3443	2518	1928	56.00	76.57	47.81
i	3857	3349	2447	63.44	73.07	51.42
j	3595	3469	2488	69.21	71.72	54.37
k	5039	3364	2728	54.14	81.09	48.07
l	3430	3489	2403	70.06	68.87	53.21

cracks. As a result, the crack segmentation quality of MSED-II is absolutely superior to that of CCE. In concrete building crack segmentation, MSED-II is superior to CCE in segmenting complete true cracks, but CCE is superior to MSED-II in segmenting correct true cracks. Thus, the performances of MSED-II and CCE in the concrete building crack segmentation are complementary.

In Table 1, there are 11 binary images with *Compl* values above 60% but merely 6 binary images in Table 3 are above 60%; even the *Compl* values of four of the binary images in Table 1 reach above 80%. A similar performance also exists in concrete building crack segmentation. In Table 2, there are 11 binary images with *Compl* values above 60%, but merely 5 binary images in Table 4 above 60%.

Table 5 indicates that MSED-II and CCE have outperformances in correctly segmenting concrete pavement and building cracks, respectively. Comparing Table 1 with Table 3, the *Corr* values derived by MSED-II are approximately higher than those by CCE. Nevertheless, the correctness performance (see Tables 2 and 4) of concrete building crack segmentation runs just contrary to the above result. MSED-II demonstrated that its correctness performance is not as good as its completeness performance, which shows absolute superiority to the completeness performance of CCE.

In the *Quality* performance, Table 5 shows that MSED-II is absolutely superior to CCE in concrete pavement crack segmentation, but is almost similar to CCE in concrete building crack segmentation. There are 9 binary images with *Quality* values above 40% in Table 1, but in Table 3 all the *Quality* values of the binary images are below 40%. Among the 24 tested inspection images, only 3 binary images were had *Quality* values approximating to or above 67% (see Table 2). A *Quality* value above 67% means that if one of the *Compl* or *Corr* value is 80%, then the other value also must reach at least 80%. Consequently, reaching a *Quality* value of 67% is really a big challenge.

5.4 Crack measurement

Each inspection image has three binary images, including M_s, S_e, and $S_e \cap M_s$. This research implemented

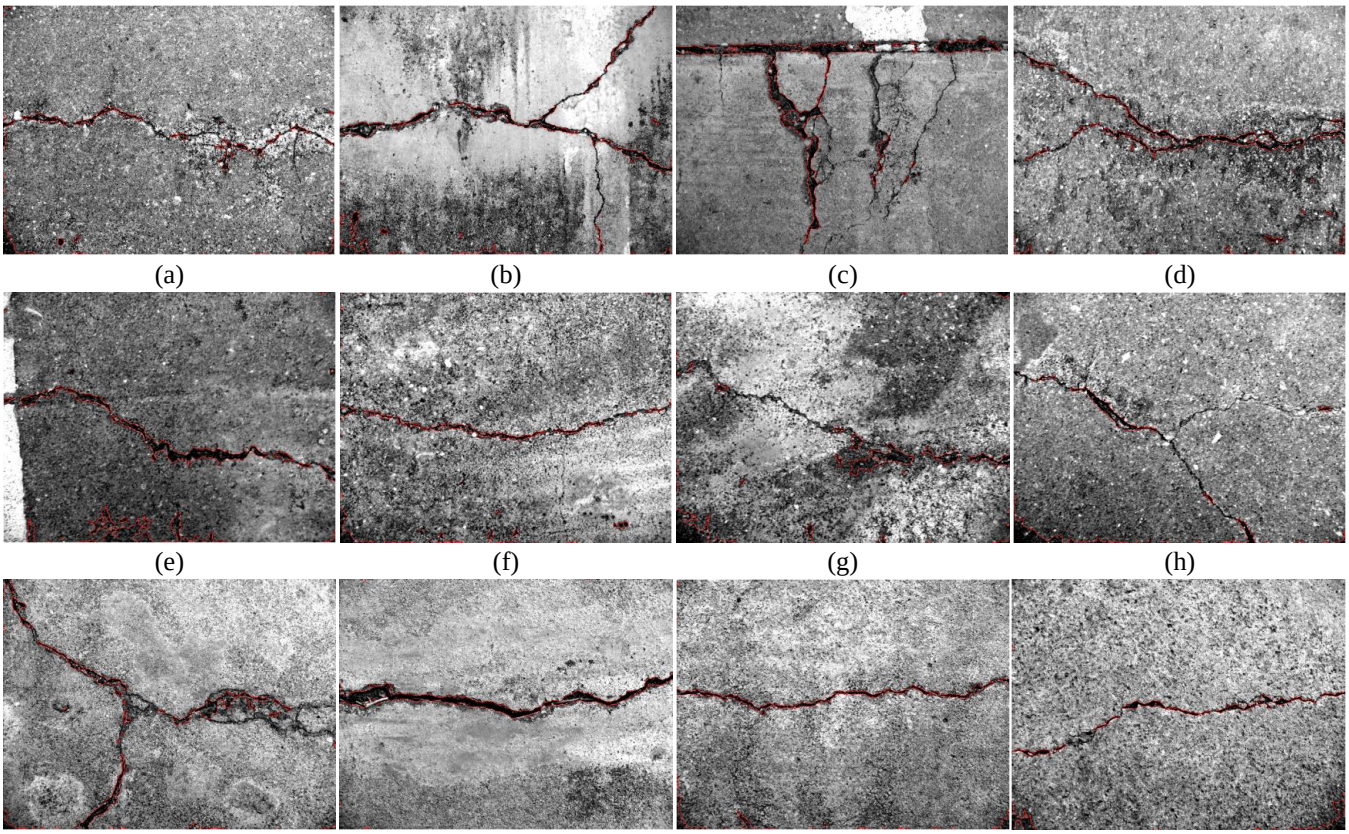

(a) (b) (c) (d)

(e) (f) (g) (h)

(i) (j) (k) (l)

Fig. 6 Segmentation result of concrete pavement cracks using MSED-II

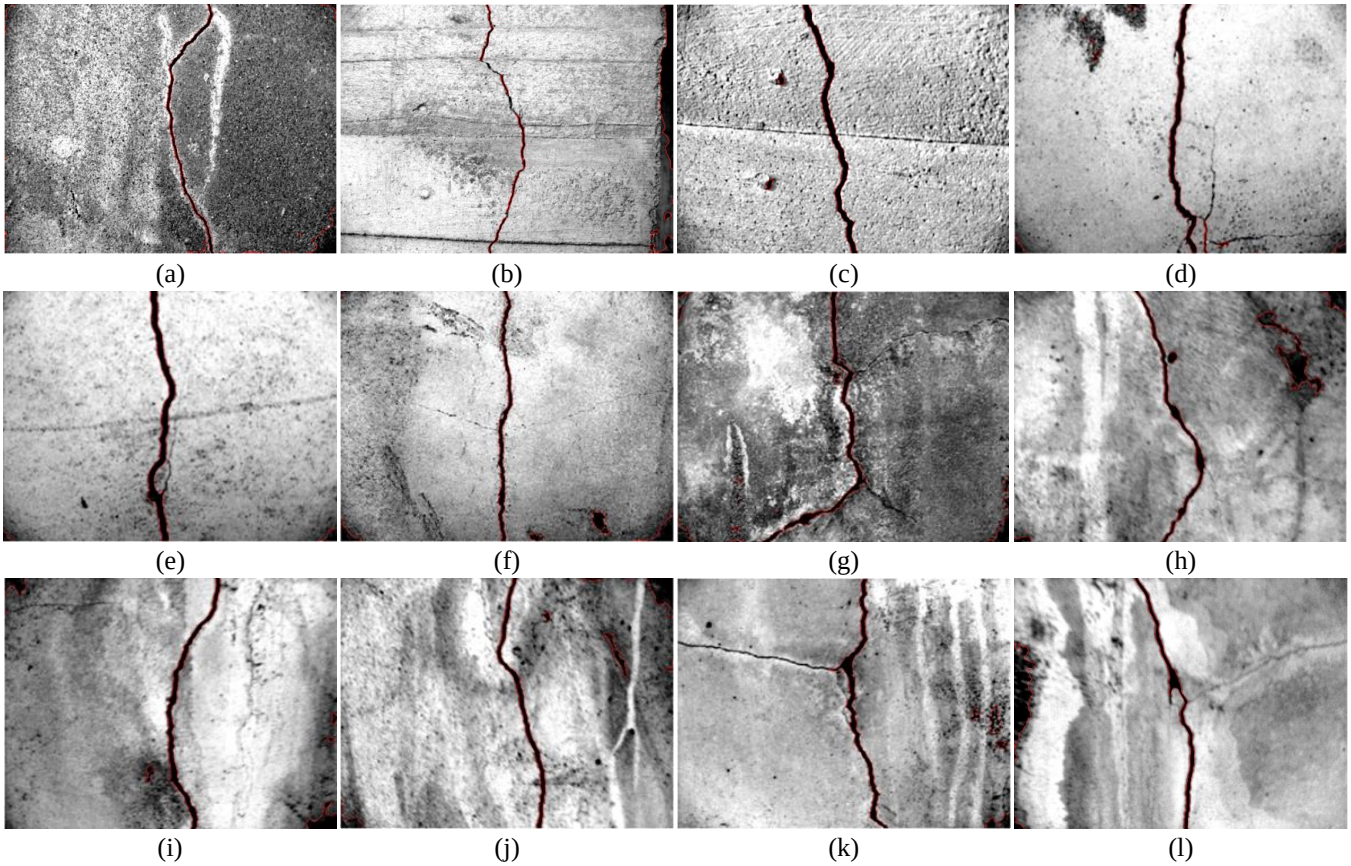

(a) (b) (c) (d)

(e) (f) (g) (h)

(i) (j) (k) (l)

Fig. 7 Segmentation result of concrete building cracks using MSED-II

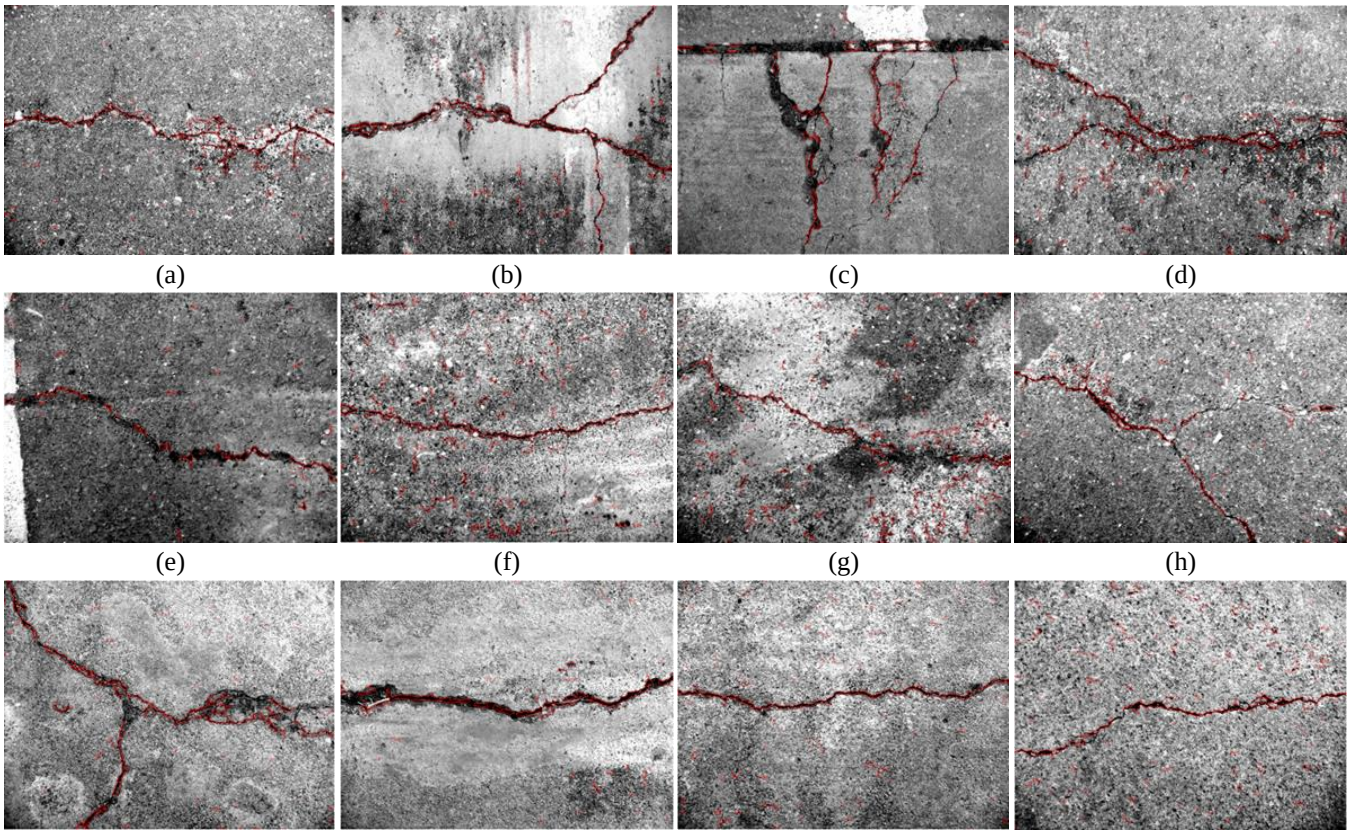

Fig. 8 Segmentation result of concrete pavement cracks using CCE

Table 5 Pair-wise comparison between MSED-II and CCE in *Compl*, *Corr*, and *Quality*

Image ID	Concrete pavement crack						Concrete building crack					
	Compl		*Corr*		*Quality*		*Compl*		*Corr*		*Quality*	
	MSED-II	CCE	MSED-II	CCE	MSED-II	CCE	MSED-II	CCE	MSED-II	CCE	MSED-II	CCE
a		√	√		√		√			√	√	
b	√		√		√		√			√		√
c	√		√		√		√		√		√	
d	√		√		√		√		√		√	
e	√			√	√		√			√	√	
f		√	√		√		√			√		√
g	√		√		√		√		√		√	
h	√			√		√	√			√		√
i	√		√		√		√			√	√	
j	√		√		√		√			√		√
k	√		√		√		√			√	√	
l	√		√		√		√			√		√

Note: The outperformance is symbolized by "√".

crack measurement based on the binary image of $S_e \cap M_s$. Only the segmented image regions belonging to true cracks were taken into consideration for crack measurement, including length, width, and area. Area means the number of pixels within the segmented image region. Length expresses the number of skeleton pixels of segmented image region. This research introduced a thinning algorithm, which can be seen in Gonzalez *et al.* (2011), into the skeleton description of the segmented image region. Area divided by length equals width, and so the calculation result represents an average width of the crack.

For each inspection image, Table 5 is a guideline for selecting a segmentation result with outperformance for *Quality* between MSED-II and CCE for crack measurement. Tables 6 and 7 show the crack measurement results based on the binary images of $S_e \cap M_s$ and M_s, respectively. The areas of true cracks have been listed in the M_s columns of either Tables 1 and 2 or Tables 3 and 4. Therefore, Table 7 merely lists the measured lengths and widths of the true cracks. Tables 6 and 7 are seen that the widths of the

Table 6 Crack measurement based on a binary image of $S_e \cap M_s$ with outperformance *Quality*

Image ID	Concrete pavement crack (pixels)			Concrete building crack (pixels)		
	Area	Length	Width	Area	Length	Width
a	1483	506	3	2010	442	5
b	3363	1008	3	1116	428	3
c	5685	2060	3	3742	429	9
d	3287	1052	3	3430	422	8
e	3414	630	5	3998	441	9
f	1708	466	4	2036	408	5
g	1676	393	4	3627	526	7
h	1420	435	3	1928	415	5
i	3023	934	3	3166	438	7
j	4564	1010	5	2488	427	6
k	1638	739	2	3390	463	7
l	1689	642	3	2403	424	6

Table 7 Crack measurement based on a binary image of M_s

Image ID	Concrete pavement crack (pixels)		Concrete building crack (pixels)	
	Length	Width	Length	Width
a	1023	2	449	7
b	1674	3	460	5
c	3451	2	436	11
d	1572	3	440	10
e	753	5	461	11
f	617	4	438	8
g	802	4	566	8
h	764	3	451	8
i	1675	3	443	9
j	1287	4	428	8
k	910	2	711	7
l	848	2	462	7

concrete pavement cracks measured by the automatic methods approximately are equal to those interpreted by human eyes. However, the automatic methods have an underestimation of 2 or 3 pixels for the width measurement of the concrete building cracks. Most of the concrete building cracks have the more pixels in width than the concrete pavement cracks, but this result does not mean that the concrete building cracks are absolutely wider than the concrete pavement cracks. In order to obtain a metric measurement result for civil engineering practices, a geometric transformation is necessary to be established in the further work. Table 8 shows an error evaluation for the crack measurement in Table 6. Here, C_{Ms} and $C_{Se\cap Ms}$ stand for one area, length, and width of a true crack and a segmented true crack, respectively. Measurement error (E) is evaluated by

$$E = (|\mathbf{C}_{Ms} - \mathbf{C}_{Se\cap Ms}| / \mathbf{C}_{Ms}) \times 100\% \quad (4)$$

The area measurement error is basically complementary to the *Compl* value. The area measurement errors of the true cracks segmented by MSED-II are approximately between 5% and 45%, but those by CCE are approximately between 30% and 55%. This result indicates that MSED-II seems to have better capability at lessening the area measurement error than does CCE.

Table 8 Error evaluation for crack measurement in Table 6

Image ID	Concrete pavement crack (%)			Concrete building crack (%)		
	Area	Length	Width	Area	Length	Width
a	39.17	50.54	50.00	32.35	1.56	28.57
b	28.11	39.78	0.00	54.67	6.96	40.00
c	30.42	40.31	50.00	19.25	1.61	18.18
d	22.99	33.08	0.00	21.64	4.09	20.00
e	7.45	16.33	0.00	21.96	4.34	18.18
f	30.74	24.47	0.00	41.38	6.85	37.50
g	45.09	51.00	0.00	20.37	7.07	12.50
h	39.50	43.06	0.00	44.00	7.98	37.50
i	31.99	44.24	0.00	17.92	1.13	22.22
j	5.68	21.52	25.00	30.79	0.23	25.00
k	10.10	18.79	0.00	32.72	34.88	0.00
l	18.05	24.29	50.00	29.94	8.23	14.29

In the length measurement, Images e and g of the concrete pavement cracks obtained the least and greatest measurement errors, respectively. The length measurement errors of the concrete pavement cracks are approximately between 15% and 50%. Among the 12 inspection images of concrete building cracks, Image k obtained a significant length measurement error of 34.88%. Excluding Image k, the length measurement errors of the concrete building cracks could be controlled under 10%. Furthermore, MSED-II and CCE seem to have a similar performance in controlling the length measurement error.

Table 8 also presents that there is an extreme difference among the width measurement errors of the concrete pavement cracks. The extreme difference is from the smaller averaged widths of the true cracks, which mostly consist of 2 through 4 pixels (see Table 7). If there is an average width difference of 1 or 2 pixels between a true crack and segmented true crack, then a width measurement error will immediately reach 25% or 50%. In addition, the width measurement errors of the concrete building cracks derived from MSED-II and CCE are approximately between 0% and 30% and between 15 and 40%, respectively. Thus, this research demonstrates that MSED-II relative to CCE can lead to a more accurate width measurement result.

6. Conclusions

This research has presented and implemented a crack enhancement algorithm, i.e. MSED-II, for segmenting and measuring crack patterns in the inspection images of concrete pavement and buildings. MSED-II based on region growing considers an 8-neighborhood connection of outlines of segmented ROIs to strengthen the morphological completeness of segmentation results. The experimental result shows that MSED-II is effective in fragmentary connection of crack segmentation to reach an extremely high completeness value of 94.32%. The experimental

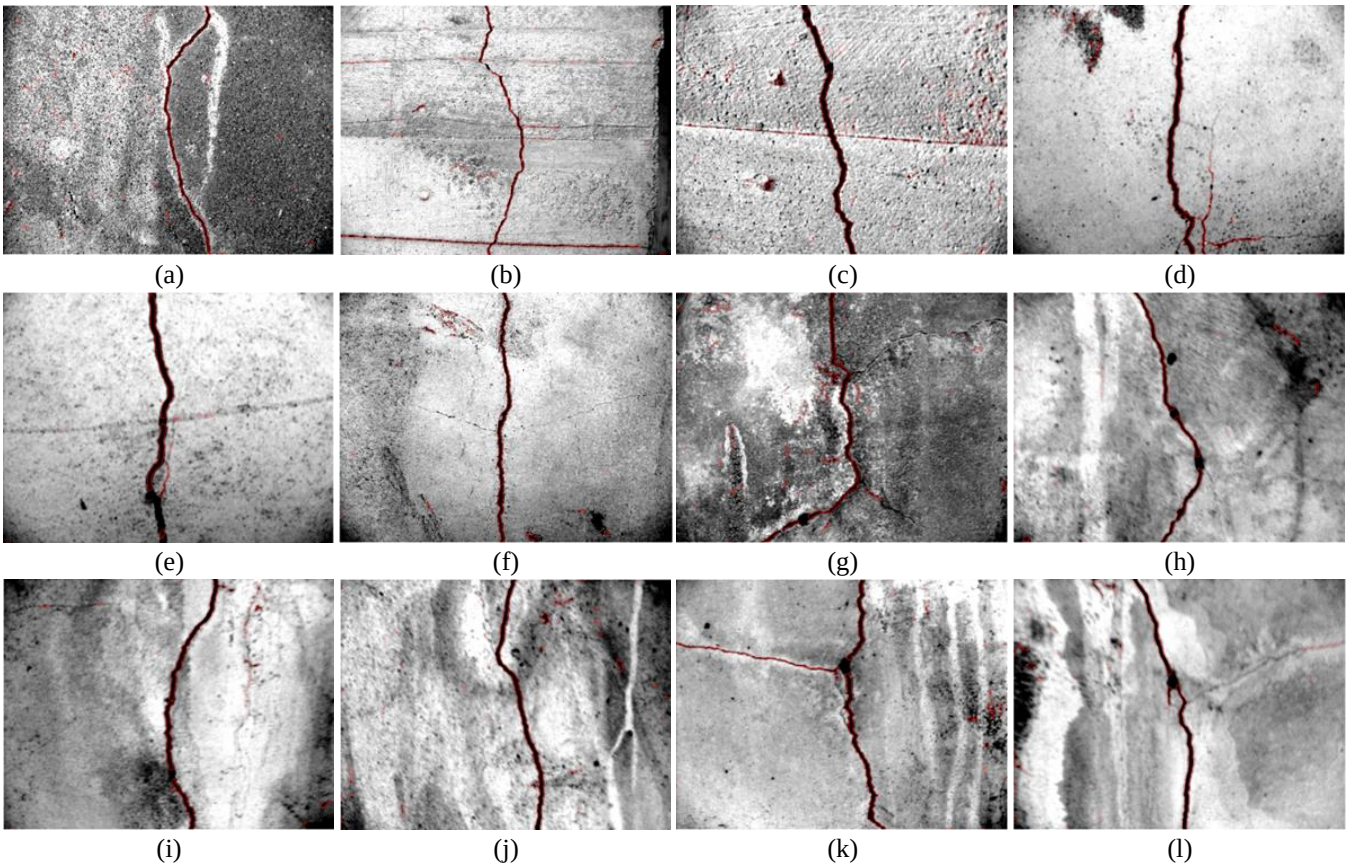

Fig. 9 Segmentation result of concrete building cracks using CCE

result of MSED-II was also compared with that of another developed crack enhancement algorithm, i.e., CCE, according to three performance indices: completeness, correctness, and quality. Generally, MSED-II can lead to a higher completeness than the correctness value, and so an improvement on background noise removal is still necessary in order to enhance crack segmentation correctness. CCE demonstrated its usefulness for obtaining a higher completeness than correctness value in concrete pavement crack segmentation, but exhibited a higher correctness than completeness value in concrete building crack segmentation. In conclusion, MSED-II relative to CCE can lead to better quality of concrete crack segmentation.

Based on a binary image with outperformance quality between MSED-II and CCE and the corresponding binary image of a true crack, the crack measurement error was also evaluated. The evaluation result indicates that MSED-II and CCE might lead to a similar length measurement error. Moreover, MSED-II relative to CCE might lead to smaller area as well as width measurement errors. In addition to CCE, MSED-II is also useful in the automatic measurement of concrete cracks. Although the obtained *Quality* values by MSED-II partially reach 67% at present, the crack segmentation results are sufficient to assist inspectors to evaluate crack sizes. If the crack segmentation correctness of MSED-II significantly rises in the future, a robust technology of automatic crack measurement can be achieved.

Acknowledgments

This research was performed partly within the project (MOST 105-2410-H-507-002) funded by the Ministry of Science and Technology, and the Higher Education Sprout Project funded by the Ministry of Education, Taiwan.

References

Belletti, B., Scolari, M. and Vecchi, F. (2017), "PARC_CL 2.0 crack model for NLFEA of reinforced concrete structures under cyclic loadings", *Comput. Struct.*, **191**,165-179.

Chen, H.J., Tai, P.H., Peng, C.F. and Yang, M.D. (2017), "Concrete crack rehabilitation using biological enzyme", *Comput. Concrete*, **19**(4), 413-417.

Chen, T., Wu, Q.H., Rahmani-Torkaman, R. and Hughes, J. (2002), "A pseudo top-hat mathematical morphological approach to edge detection in dark regions", *Pattern Recognit.*, **35**(1), 199-210.

Gokhale, S. and Graham, J.A. (2004), "A new development in locating leaks in sanitary sewers", *Tunn. Undergr. Space Technol.*, **19**(1), 85-96.

Gonzalez, R.C., Woods, R.E. and Eddins, S.L. (2011), *Digital Image Processing Using Matlab*, 2nd Edition, McGraw-Hill, USA.

Iyer, S. and Sinha, S.K. (2005), "A robust approach for automatic detection and segmentation of cracks in underground pipeline images", *Image Vis. Comput.*, **23**(10), 921-933.

Janowski, A., Nagrodzka-Godycka, K., Szulwic, J. and Ziolkowski, P. (2016), "Remote sensing and photogrammetry

techniques in diagnostics of concrete structures", *Comput. Concrete*, **18**(3), 405-420,

Lee, J.H., Yoo, H.S., Kim, Y.S., Lee, J.B. and Cho, M.Y. (2006), "The development of a machine vision-assisted, teleoperated pavement crack sealer", *Autom. Constr.*, **15**(5), 616-626.

Mashford, J., Rahilly, M., Davis, P. and Burn, S. (2010), "A morphological approach to pipe image interpretation based on segmentation by support vector machine", *Autom. Constr.*, **19**(7), 875-883.

Metni, N. and Hamel, T. (2007), "A UAV for bridge inspection: Visual serving control law with orientation limits", *Automat. Constr.*, **17**(1), 3-10.

Oh, J.K., Jang, G., Oh, S., Lee, J.H., Yi, B.J., Moon, Y.S., Lee, J.S. and Choi, Y. (2009), "Bridge inspection robot system with machine vision", *Automat. Constr.*, **18**(7), 929-941.

Pan, N.F., Ko, C.H., Yang, M.D. and Hsu, K.C. (2011), "Pavement performance prediction through fuzzy regression", *Exp. Syst. Appl.*, **38**(8), 10010-10017.

Riveiro, B., Jauregui, D.V., Arias, P., Armesto, J. and Jiang, R. (2012), "An innovative method for remote measurement of minimum vertical under clearance in routine bridge inspection", *Autom. Constr.*, **25**, 34-40.

Shih, F.Y. (2010). Image Processing and Pattern Recognition, Wiley, New Jersey.

Sinha, S.K. and Fieguth, P.W. (2006), "Segmentation of buried concrete pipe images", *Autom. Constr.*, **15**(1), 47-57.

Su, T.C. (2013), "Application of computer vision to crack detection of concrete structure", *IACSIT Int. J. Eng. Technol.*, **5**(4), 457-461.

Su, T.C. (2015), "Segmentation of crack and open joint in sewer pipelines based on CCTV inspection images", *ACSR-Adv. in Comput. Sci. Res.*, **9**, 263-266.

Su, T.C. and Yang, M.D. (2014), "Application of morphological segmentation to leaking defect detection in sewer pipelines", *Sensors.*, **14**(5), 8686-8704.

Su, T.C., Yang, M.D., Wu, T.C. and Lin, J.Y. (2011), "Morphological segmentation based on edge detection for sewer pipe defects on CCTV images", *Expert Syst. Appl.*, **38**(10), 13094-13114.

Sun, L., Kamaliardakani, M. and Zhang, Y.M. (2016), "Weighted neighborhood pixels segmentation method for automated detection of cracks on pavement surface images", *J. Comput. Civil. Eng.*, **30**(2).

Tung, P.C., Hwang, Y.R. and Wu, M.C. (2002), "The development of a mobile manipulator imaging system for bridge crack inspection", *Autom. Constr.*, **11**(6), 717-729.

Victores, J.G., Martínez, S., Jardón, A. and Balaguer, C. (2011), "Robot-aided tunnel inspection and maintenance system by vision and proximity sensor integration", *Autom. Constr.*, **20**(5), 629-636.

Wang, T.T., Jaw, J.J., Chang, Y.H. and Jeng, F.S. (2009), "Application and validation of profile-image method for measuring deformation of tunnel wall", *Tunn. Undergr. Space Technol.*, **24**(2), 136-147.

Wendt, P.D., Coyle, E.J. and Gallagher, N.C. (1986), "Stack filters", *IEEE Trans. Acoust. Speech Signal Pr.*, **34**(4), 898-911.

Yan, H. (1996), "Unified formulation of a class of image thresholding techniques", *Pattern Recogn.*, **29**(12), 2025-2032.

Yang, M.D. and Su, T.C. (2006), "Automation model of sewerage rehabilitation planning", *Water Sci. Technol.*, **54**(11-12), 225-232,

Yang, M.D. and Su, T.C. (2007), "An optimization model of sewerage rehabilitation", *J. Chin. Inst. Eng.*, **30**(4), 651-659.

Yang, M.D. and Su, T.C. (2008), "Automated diagnosis of sewer pipe defects based on machine learning approaches", *Exp. Syst. Appl.*, **35**(3), 1327-1337.

Yang, M.D. and Su, T.C. (2009), "Segmenting ideal morphologies of sewer pipe defects on CCTV images for automated diagnosis", *Exp. Syst. Appl.*, **36**(2), 3562-3573.

Yang, M.D., Chen, Y.P., Su, T.C. and Lin, Y.H. (2017), "Sewer pipe defects diagnosis assessment using multivariate analysis on CCTV video imagery", *Urban. Water J.*, **14**(5), 475-482.

Yang, M.D., Lin, M.D., Lin, Y.H. and Tsai, K.T. (2017), "Multiobjective optimization design of green building envelope material using a non-dominated sorting genetic algorithm", *Appl. Therm. Eng.*, **111**, 1255-1264.

Yang, M.D., Su, T.C., Pan, N.F. and Liu, P. (2011a), "Feature extraction of sewer pipe defects using wavelet transform and co-occurrence matrix", *Int. J. Wavelets Multi.*, **9**(2), 211-225.

Yang, M.D., Su, T.C., Pan, N.F. and Yang, Y.F. (2011b), "Systematic image quality assessment for sewer inspection", *Exp. Syst. Appl.*, **38**(3), 1766-1776.

Yang, S.T., Li, K.F. and Li, C.Q. (2017), "Numerical determination of concrete crack width for corrosion-affected concrete structures", *Comput. Struct..*, https://doi.org/10.1016/j.compstruc.2017.07.016.

Yli-Harja, O., Astola, J. and Neuvo, Y. (1991), "Analysis of the properties of median and weighted median filters using threshold logic and stack filter representation", *IEEE Trans. Signal Pr.*, **39**(2), 395-410.

Yu, S.N., Jang, J.H. and Han, C.S. (2007), "Auto inspection system using a mobile robot for detecting concrete cracks in a tunnel", *Autom. Constr.*, **16**(3), 255-261.

Yun, H.B., Mokhtari, S. and Wu, L.L. (2015), "Crack recognition and segmentation using morphological image-processing techniques for flexible pavements", *Transp. Res. Rec.*, **2523**, 115-124.

Zhu, Z., German, S. and Brilakis, I. (2010), "Detection of large-scale concrete columns for automated bridge inspection", *Autom. Constr.*, **19(**8), 1047-1055.

CC